

Nuclear landscape in covariant density functional theory.

A. V. Afanasjev^{a,*}, S. E. Abgemava^a, D. Ray^a, P. Ring^b

^aDepartment of Physics and Astronomy, Mississippi State University, MS 39762

^bFakultät für Physik, Technische Universität München, D-85748 Garching, Germany

Abstract

The neutron and proton drip lines represent the limits of the nuclear landscape. While the proton drip line is measured experimentally up to rather high Z -values, the location of the neutron drip line for absolute majority of elements is based on theoretical predictions which involve extreme extrapolations. The first ever systematic investigation of the location of the proton and neutron drip lines in the covariant density functional theory has been performed by employing a set of the state-of-the-art parametrizations. Calculated theoretical uncertainties in the position of two-neutron drip line are compared with those obtained in non-relativistic DFT calculations. Shell effects drastically affect the shape of two-neutron drip line. In particular, model uncertainties in the definition of two-neutron drip line at $Z \sim 54, N = 126$ and $Z \sim 82, N = 184$ are very small due to the impact of spherical shell closures at $N = 126$ and 184 .

Keywords: Proton and neutron drip lines, covariant density functional theory, two-particle separation energies

At present, the nuclear masses of approximately 3000 out of roughly 7000 nuclei expected between nuclear drip lines are known [1]. Nuclear existence ends at the drip lines. While the proton drip line has been delineated in experiment up to protactinium ($Z = 91$), the position of the neutron drip line beyond $Z = 8$ is determined only in model calculations. Different models and different parameterizations show rather large variations in predictions of the neutron drip line. Moreover, because of experimental limitations even in foreseeable future it will be possible to define the location of neutron-drip line for the majority of elements only in model calculations. In such a situation it is important to estimate the errors in the location of the predicted neutron drip line introduced by the use of the various calculations. In this context we have to distinguish the results and related theoretical uncertainties obtained within the same model, but with different parameterizations and the results and uncertainties obtained with different models.

Theoretical uncertainties(errors) in the prediction of physical observables have several sources of origin. Within one class of models they are the consequences of specific assumptions and the optimization protocols. The differences in the basic assumptions of different model classes is another source. They lead to theoretical uncertainties which can be revealed only by a systematic comparison of a variety of models.

The first attempt to estimate theoretical uncertainties in the definition of two-neutron drip line within one class of models has been performed within the Skyrme density functional theory (SDFT) in Ref. [2] employing the set of six parametrizations. These results were compared with those obtained in other classes of non-relativistic models such as the microscopic-macroscopic finite range droplet model (FRDM) [3] and the

Skyrme Hartree-Fock-Bogoliubov (HFB) calculations of Ref. [4] with the HFB-21 parametrization. It turns out that the two-neutron drip lines of the FRDM and Skyrme-HFB calculations are located either within the SDFT error band or very close to it. Similar calculations exist also for non-relativistic DFT models based on the finite range Gogny forces D1S [5] and D1M [6].

The question of theoretical errors in the definition of the neutron drip line is still not resolved since the important class of nuclear structure models known under name covariant density functional theory (CDFT) [7, 8, 9, 10, 11] has not been applied so far in a reliable way to the study of this quantity. Typically, non-relativistic and relativistic DFT differ significantly in the prediction of separation energies close to the drip lines and, in general, of isovector properties far from stability [12]. This may lead to neutron drip lines which differ substantially from non-relativistic models. The goals of the present manuscript are (i) the systematic study of two-proton- and two-neutron-drip lines within the relativistic Hartree-Bogoliubov (RHB) framework [13, 14] using several state-of-the-art CDFT parametrizations, (ii) the estimate of theoretical errors in the location of the drip lines within CDFT framework, and (iii) the comparison of the drip lines obtained in relativistic and non-relativistic DFT and thus the estimate of global theoretical errors.

To our knowledge, there were only two previous attempts to study the neutron-drip line in the CDFT framework [15, 16]. However, both of them employ quite crude approximations to the physics of drip line nuclei with a rather limited validity. For example, the pairing correlations have been completely ignored in the studies of Ref. [15] and the treatment of pairing via BCS approximation in Ref. [16] is questionable in the region of drip line since this approximation does not take into account the continuum properly and leads to the formation of a neutron gas [17] in nuclei near neutron-drip line. In addition, these calcula-

*Corresponding author

Email address: afanasjev@erc.msstate.edu (A. V. Afanasjev)

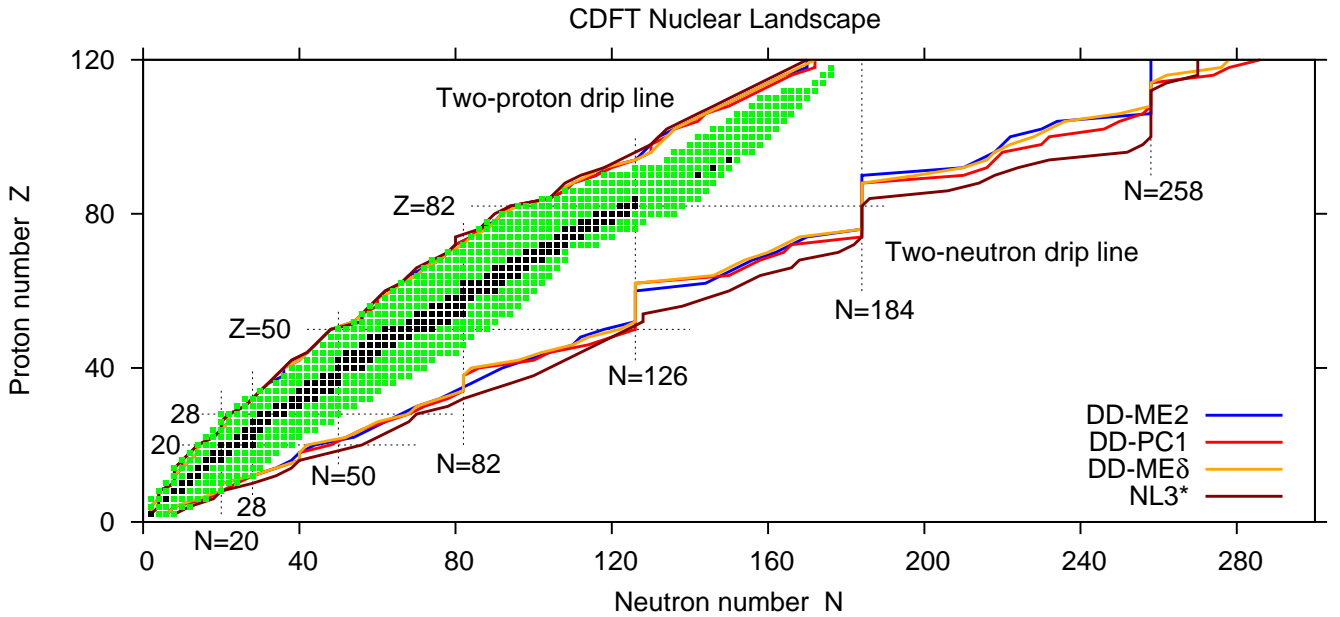


Figure 1: The landscape of bound even-even nuclei as obtained in the CDFT calculations. Experimentally known stable and radioactive nuclei are shown by black and green squares, respectively. The experimental data are from Ref. [1]. Two-proton and two-neutron drip lines calculated with different CEDF are shown by the lines of different color.

tions use at most 14 fermionic shells for the harmonic oscillator basis, which according to our study and the one of Ref. [18] is not sufficient for a correct description of binding energies of actinides and superheavy nuclei and the nuclei in the vicinity of neutron-drip line. The RHB framework with a finite range pairing force is a proper tool for that purpose. It has been applied very successfully with the parameter set NL3 [19, 20] and the parameter set DD-PC1 [21] at the proton drip line and it has the proper coupling to the continuum at the neutron drip line.

In the present manuscript, the RHB framework is used for a systematic studies of ground state properties of all even-even nuclei from the proton- to neutron drip line. The separable version [22, 23] of the finite range Brink-Booker part of the Gogny D1S force is used in the particle-particle channel; its strength variation across the nuclear chart is defined by means of the fit of rotational moments of inertia calculated in the cranked RHB framework to experimental data via the procedure of Ref. [24]. The need for such A -dependent variation of the strength of the Brink-Booker part of the Gogny D1S force in the CDFT application has recently been discussed in Refs. [24, 25]. As the absolute majority of nuclei are known to be axially and reflection symmetric in their ground states, we consider only axial and parity-conserving intrinsic states and solve the RHB-equations in an axially deformed oscillator basis [26, 27]. The truncation of the basis is performed in such a way that all states belonging to the shells up to $N_F = 20$ fermionic shells and $N_B = 20$ bosonic shells are taken into account. This provides sufficient numerical accuracy. As the absolute majority of nuclei are known to be axially and reflection symmetric in their ground states, we consider only axial and parity-conserving intrinsic states. For each nucleus the potential energy curve in large deformation range from $\beta_2 = -0.4$ up to $\beta_2 = 1.0$ is ob-

tained by means of constraint on the quadrupole moment Q_{20} . Then, the correct ground state configuration and its energy are defined; this procedure is especially important for the cases of shape coexistence.

In axial reflection-symmetric calculations for superheavy nuclei with $Z \geq 100$, the superdeformed minimum is frequently lower in energy than the normal deformed one [28]. As long as triaxial and octupole deformations are not included, this minimum is stabilized by the presence of an outer fission barrier. Including such deformations, however, it often turns out that this minimum either disappears or becomes a saddle point, unstable against fission [28]. Since these deformations are not included in the present calculations, we restrict our consideration to spherical or normal-deformed ground states in the $Z \geq 100$ nuclei. This also facilitates the comparison with non-relativistic results which favor such ground states for these nuclei.

Three existing classes of covariant density functional models are used throughout this paper: the nonlinear meson-nucleon coupling model (NL), the density-dependent meson-exchange model (DD-ME), and a density-dependent point coupling model (DD-PC); see their comparison in Ref. [28]. The main differences among them lay in the treatment of the range of the interaction, the mesons, and the density dependence. The interaction in the first two classes has a finite range, while the third class uses a zero-range interaction with one additional gradient term in the scalar-isoscalar channel. The mesons are absent in the density-dependent point coupling model. The density dependence is explicit in the last two models, while it shows up via the nonlinear meson-couplings in the first case.

Each of these model classes is represented here by the energy density functional (EDF) that is considered to be the state-of-the-art. The NL model is represented here by the NL3* [29]

EDF which has the smallest number of parameters amongst considered EDF fitted to data. The DD-ME model is represented by the DD-ME2 [30] and the DD-ME δ [31] EDFs. The DD-ME δ EDF differs from others by the inclusion of the δ -meson, which leads to different proton and neutron effective masses. In addition, the parameters of the DD-ME δ EDF are largely based on microscopic *ab initio* calculations in nuclear matter; only four of its parameters are fitted to finite nuclei. On the contrary, all parameters of other EDF were adjusted to experimental data based on the properties of finite nuclei. The DD-PC model is represented by the DD-PC1 [32] EDF. In contrast to the other functionals, which are fitted to spherical nuclei, this EDF is fitted to a large set of deformed nuclei.

Fig. 1 shows the nuclear landscape as obtained with these CDFT parametrizations. The particle stability (and, as a consequence, a drip line) of a nuclide is specified by its separation energy, namely, the amount of energy needed to remove particle(s). Since our investigation is restricted to even-even nuclei, we consider two-neutron $S_{2n} = B(Z, N - 2) - B(Z, N)$ and two-proton $S_{2p} = B(Z - 2, N) - B(Z, N)$ separation energies. Here $B(Z, N)$ stands for the binding energy of a nucleus with Z protons and N neutrons. If the separation energy is positive, the nucleus is stable against two-nucleon emission; conversely, if the separation energy is negative, the nucleus is unstable. Thus, two-neutron and two-proton drip lines are reached when $S_{2n} \leq 0$ and $S_{2p} \leq 0$, respectively.

Table 1: The rms-deviations ΔE_{rms} , $\Delta(S_{2n})_{rms}$ ($\Delta(S_{2p})_{rms}$) between calculated and experimental binding energies E and two-neutron(-proton) separation energies S_{2n} (S_{2p}), respectively. They are given in MeV for indicated CDFT parametrizations with respect of “measured” and “measured+estimated” sets of experimental masses.

EDF	measured	measured+estimated		
	ΔE_{rms}	ΔE_{rms}	$\Delta(S_{2n})_{rms}$	$\Delta(S_{2p})_{rms}$
NL3*	2.97	3.01	1.21	1.28
DD-ME2	2.42	2.48	1.09	0.99
DD-ME δ	2.31	2.42	1.11	1.11
DD-PC1	2.02	2.17	1.25	1.13

The accuracy of the description of separation energies depend on the accuracy of the description of mass differences. The global RHB calculations of masses with employed parametrizations lead to the rms-deviations ΔE_{rms} between calculated and experimental binding energies which are listed in Table 1. The detailed results of these calculations will be presented in a forthcoming manuscript [33]. The masses given in the AME2012 mass evaluation [1] can be separated into two groups; one represents nuclei with masses defined only from experimental data, the other contains nuclei with masses depending in addition on either interpolation or extrapolation procedures. For simplicity, we call the masses of the nuclei in the first and second groups as measured and estimated. There are 640 measured and 195 estimated masses of even-even nuclei in the AME2012 mass evaluation. One can see in Table 1 that the addition of estimated masses leads only to a slight decrease of the accuracy of the description of experimental data. Two-neutron S_{2n} and two-proton S_{2p} separation energies are

described with typical accuracy of 1 MeV (Table 1). One can see that not always the parametrization which provides the best description of masses gives the best description of two-particle separation energies. This is because the separation energies are related to the derivatives of binding energies with respect of particle number.

Fig. 2 shows that theoretical uncertainties (i. e. the spread of the predictions due to different EDF) are rather small for two-proton drip line. In addition, the results of the calculations are very close to experimental data. This is because the proton-drip line lies close to the valley of stability, so that extrapolation errors towards it are small. Another reason is the fact the Coulomb barrier provides a rather steep potential reducing considerably the coupling to the proton continuum. This leads to a relatively low density of the single-particle states in the vicinity of the Fermi level.

The situation is different for the two-neutron drip line. In the majority of the cases, the theoretical uncertainties in the location of this line are much larger than for the two-proton drip one and they are generally increasing with the increase of mass number. This is commonly attributed to poorly known isovector properties of EDF [2]. Although this factor contributes, such an explanation is somewhat oversimplified from our point of view. That is because for some combinations of Z and N there is basically no (or very little) dependence of the predictions for the location of the two-neutron drip line on the CDFT parametrization. Such a weak (or vanishing) dependence is especially pronounced at spherical neutron shell closures with $N = 126, 184$ and 258 around proton numbers $Z = 54, 80$ and 110 . It is interesting that the impact of shell structure at these particle numbers on the shape of the two-neutron drip line is more pronounced than that for the two-proton drip line due to $Z = 50$ and 82 proton shell gaps.

However, moving away from these spherical shell closures the spread of theoretical predictions for the two-neutron drip line increases. This move also induces the deformation in the nuclei. Thus, there is a close correlation between the nuclear deformation at the neutron-drip line and the uncertainties in the prediction of neutron-drip line; the regions of large uncertainties corresponds to transitional and deformed nuclei. This is caused by the underlying densities of the single-particle states. The spherical nuclei under discussion are characterized by large shell gaps and a clustering of highly degenerate single-particle states around them. Deformation removes this high degeneracy of single-particle states and leads to a more equal distribution of the single-particle states with energy. Moreover, the density of bound neutron single-particle states close to the neutron continuum is substantially larger than that on the proton-drip line. As a consequence, inevitable inaccuracies in the DFT description of the deformed single-particle state energies which are present even in the valley of beta-stability [34] will lead to larger uncertainties in the predictions of the neutron-drip line.

For some isotope chains, there are regions of two-neutron stability (not shown in Fig. 1) at neutron numbers beyond the primary two-neutron drip line. The physical mechanism behind the appearance of these regions is illustrated in Fig. 3 on the example of the Th isotope chain. Two-neutron separation

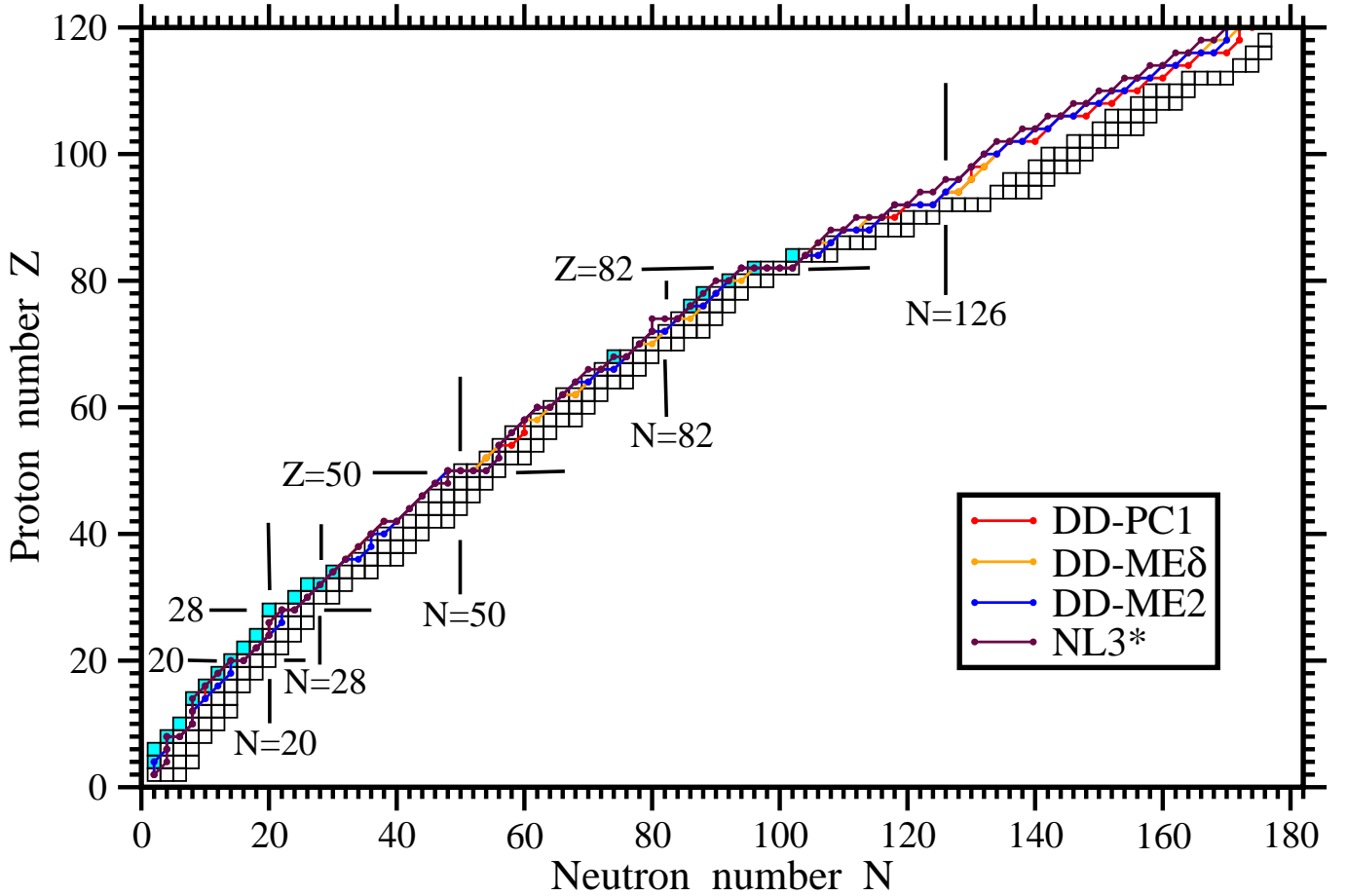


Figure 2: Calculated versus experimental two-proton drip lines. For each isotope chain, the four experimentally known most proton-rich nuclei are shown by squares. Cyan shading of the squares is used for the nuclei located beyond the two-proton drip line ($S_{2p} < 0$). The borderline between shaded and open squares delineates known two-proton drip line. Only in the case of the $Z = 4, 6, 8, 80, 82$ and 84 isotope chains, the location of two-proton drip line is firmly established since the masses of the nuclei on both sides of the drip line are directly and accurately measured. The two-proton drip line is only tentatively delineated for the $Z = 10, 14 - 34, 68, 76$ and 78 chains since the masses of beyond the drip line nuclei are only estimated in Ref. [1]. The lines with small symbols show the calculated two-proton drip lines which go along the last two-proton bound nuclei.

energies S_{2n} and the neutron chemical potential λ_{2n} are positive and negative in two-neutron bound nuclei ($N \leq 184$), respectively. The S_{2n} and λ_{2n} values become negative and positive for two-neutron unbound nuclei ($186 \leq N \leq 192$), respectively. A further increase of the neutron number triggers an increase of quadrupole deformation β_2 leading to a lowering of the neutron chemical potential λ_n which again becomes negative. As a consequence, two-neutron binding reappears ($S_{2n} > 0$) at $N = 194 - 206$. Further increase of N beyond 206 leads to two-neutron unbound nuclei. The appearance of these regions, however, strongly depends on the CDFT parametrization. For example, such regions exist at ($Z = 62, N = 132 - 146$), ($Z = 88, N = 194 - 206$) for DD-PC1, at ($Z = 74, N = 176 - 184$), ($Z = 90, N = 194 - 206$) for DD-ME2 and at ($Z = 62, N = 132 - 142$), ($Z = 74, N = 178 - 184$) and ($Z = 90, N = 204 - 206$) for DD-ME δ . However, the regions of stability beyond the primary drip line are absent in the RHB(NL3*) calculations.

A similar reappearance of two-neutron binding with increasing neutron number beyond primary two-neutron drip line ex-

ists also in many SDFT parametrizations [2]. Both in CDFT and SDFT, the regions of two-neutron binding reappearance represent the peninsulas emerging from the nuclear mainland. Ref. [2] suggested that such behavior is due to the presence of shell effects at neutron closures that tend to lower binding energy along the localized bands of stability. This is certainly true in some cases. However, our analysis presented above suggests that local changes of the shell structure induced by deformation changes play also an important role. Similar to the CDFT(NL3*) results, there are also some Skyrme EDF which do not show the reappearance of two-neutron binding [35].

It is interesting to compare theoretical CDFT uncertainties in the definition of the two-proton and two-neutron drip lines with the ones obtained in non-relativistic calculations. Fig. 4 presents such a comparison. We use so-called '2012 Benchmark uncertainties' [35] obtained in Ref. [2] for Skyrme DFT employing six parametrizations; these uncertainties are shown by the combination of yellow and blue shaded areas in Fig. 4. The CDFT uncertainties are represented by the combination of the plum and blue shaded areas. One can see that the CDFT

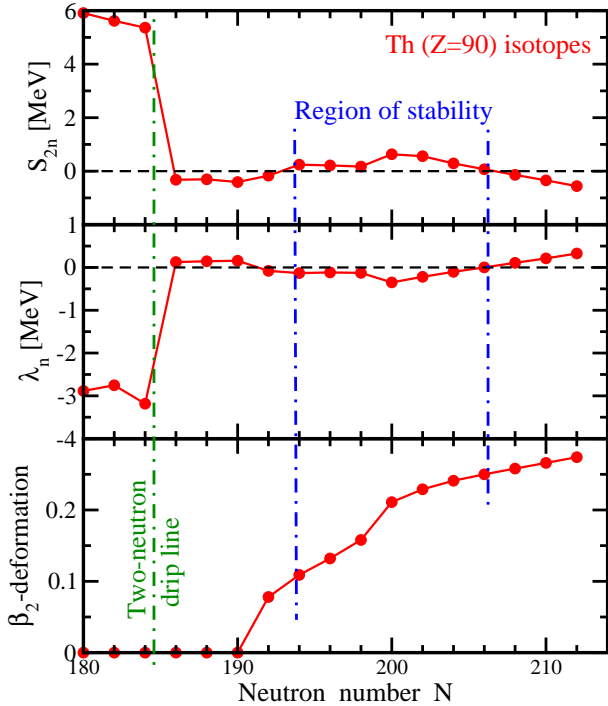


Figure 3: Two-neutron separation energies S_{2n} , neutron chemical potentials λ_n , and quadrupole deformations β_2 of the Th ($Z = 90$) isotopes obtained in the RHB(DD-ME2) calculations.

and SDFT uncertainties in the definition of two-proton drip line are small; they tightly overlap at $Z \leq 70$ while for higher Z the CDFT uncertainties are shifted slightly towards neutron deficient nuclei as compared with the SDFT ones. The uncertainties for two-neutron drip line are larger but still they are similar in two models in many regions. In particular, the two-neutron drip line at $Z \sim 54, N = 126$ and $Z \sim 82, N = 184$ is well defined not only in the CDFT and SDFT calculations, but also in the mic+mac (FRDLM) and Gogny D1S calculations. This uniqueness is due to corresponding well pronounced spherical shell closures in the model calculations.

The predictions of the DD-ME2, DD-ME δ and DD-PC1 parametrizations are close to each other (Fig. 1) and are within the '2012 Benchmark uncertainties'. The NL3* parametrization typically shifts the two-neutron drip line to a higher N -value exceeding in some regions '2012 Benchmark uncertainties'. However, the same is true for recently fitted Skyrme TOVmin parametrization [35], the two-neutron drip line of which is very similar to the one obtained in the RHB(NL3*) calculations.

The biggest difference between CDFT and Skyrme DFT calculations appears at $N = 258, Z \sim 110$ (see Fig. 4) where the two-neutron drip line is uniquely defined in the CDFT calculations due to large spherical gap at $N = 258$. This gap is also present in many Skyrme EDF but it does not prevent a significant spread of Skyrme DFT predictions for the two-neutron drip line in this region. This again underlines the importance of shell structure in the predictions of the details of the two-neutron drip line. A similar difference between CDFT and SDFT exists also

in superheavy nuclei with $Z \approx 120 - 126, N \approx 172 - 184$ where different centers of islands of stability are predicted by these models [36, 37]. These results are contrary to the fact that both models generally agree for lighter $Z \leq 100$ nuclei.

The DD-* CEDF predict two-neutron drip line at lower N as compared with the NL3* one (see Fig. 1). It is tempting to associate this feature with different symmetry energies J ($J \sim 32$ MeV for DD* and $J \sim 39$ MeV for NL3*). However, a detailed analysis of 14 two-neutron drip lines obtained in relativistic and non-relativistic calculations does not reveal clear correlations between the location of two-neutron drip line and the nuclear matter properties of the employed force.

In conclusion, a detailed analysis of two-neutron drip lines in covariant and non-relativistic DFT has been performed. These results clearly indicate that the shell structure is not washed near or at two-neutron drip line. In particular, model uncertainties in the definition of two-neutron drip line at $Z \sim 54, N = 126$ and $Z \sim 82, N = 184$ are very small due to the impact of spherical shell closures at $N = 126$ and 184 . The largest difference between covariant and Skyrme DFT exist in superheavy nuclei, where the first model (contrary to second) predicts significant impact of the $N = 258$ spherical shell closure. The spread of theoretical predictions grows up on moving away from these spherical closures. The development of deformation causes it. Both poorly known isovector properties of the forces and inevitable inaccuracies in the description of deformed single-particle states in the DFT framework contribute to that. The number of particle-bound even-even $Z \leq 120$ nuclei is 2040, 2050, 2057 and 2216 in the DD-PC1, DD-ME2, DD-ME δ and NL3* parametrizations, respectively. This is close to the numbers obtained in SDFT. Thus, our calculations support the estimate of Ref. [2] that around 7000 different (including odd- and odd-odd ones) nuclides have to exist.

The authors would like to thank J. Erler for valuable discussions. This work has been supported by the U.S. Department of Energy under the grant DE-FG02-07ER41459 and by the DFG cluster of excellence "Origin and Structure of the Universe" (www.universe-cluster.de). This research was also supported by an allocation of advanced computing resources provided by the National Science Foundation. The computations were partially performed on Kraken at the National Institute for Computational Sciences (<http://www.nics.tennessee.edu/>).

References

- [1] M. Wang, G. Audi, A. H. Wapstra, F. G. Kondev, M. MacCormick, X. Xu and B. Pfeiffer, *Chinese Physics C* **36**, 1603 (2012).
- [2] J. Erler, N. Birge, M. Kortelainen, W. Nazarewicz, E. Olsen, A. M. Perhac, M. Stoitsov, *Nature* **486**, 509 (2012).
- [3] P. Möller, J. R. Nix, W. D. Myers, W. J. Swiatecki, *At. Data Nucl. Data Tabl.* **59**, 185 (1995).
- [4] S. Goriely, N. Chamel and J. M. Pearson, *Phys. Rev. C* **82**, 035804 (2010).
- [5] J.-P. Delaroche, M. Girod, J. Libert, H. Goutte, S. Hilaire, S. Peru, N. Pillet, and G. F. Bertsch, *Phys. Rev. C* **81**, 014303 (2010).
- [6] S. Goriely, S. Hilaire, M. Girod, and S. Péru, *Phys. Rev. Lett.* **102**, 242501 (2009).
- [7] B. D. Serot and J. D. Walecka, *Adv. Nucl. Phys.* **16**, 1 (1986).
- [8] P.-G. Reinhard, *Rep. Prog. Phys.* **52**, 439 (1989).
- [9] P. Ring, *Prog. Part. Nucl. Phys.* **37**, 193 (1996).

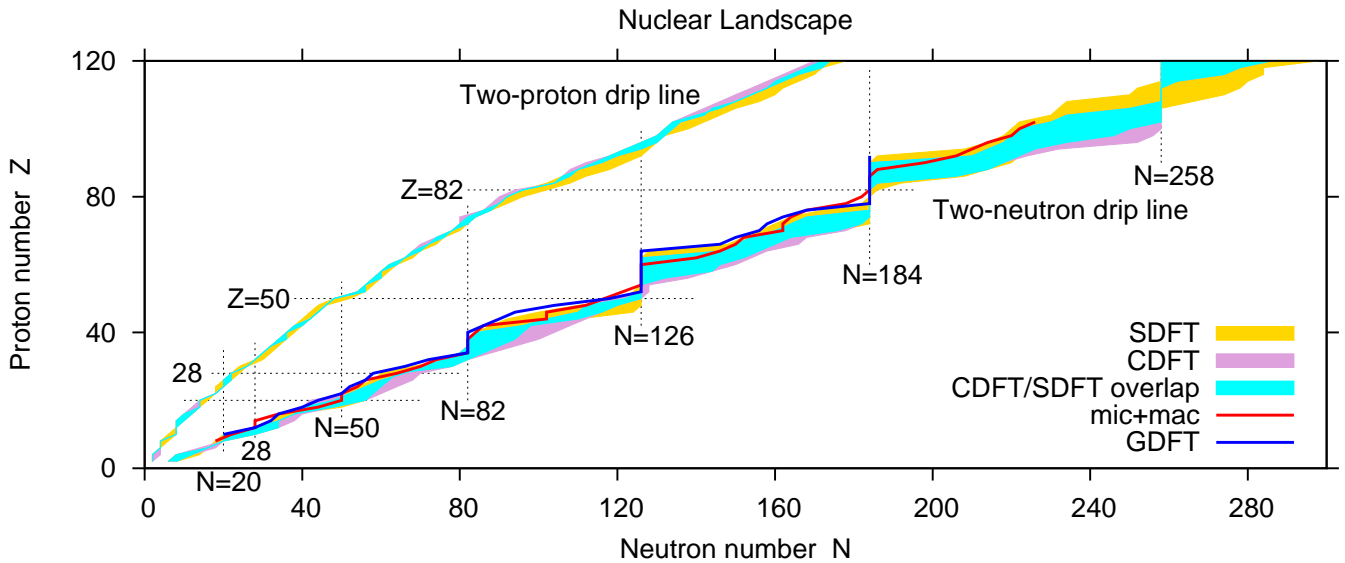


Figure 4: The comparison of the uncertainties in the definition of two-proton and two-neutron drip lines obtained in CDFT and SDFT. The shaded areas are defined by the extremes of the predictions of the corresponding drip lines obtained with different parametrizations. The blue shaded area shows the area where the CDFT and SDFT results overlap. Non-overlapping regions are shown by dark yellow and plum colors for SDFT and CDFT, respectively. The results of the SDFT calculations are taken from the supplement to Ref. [2]. The two-neutron drip lines obtained by microscopic+macroscopic (FRDM [3]) and Gogny D1S DFT [5] calculations are shown by red and blue lines, respectively.

- [10] D. Vretenar, A. V. Afanasjev, G. A. Lalazissis, and P. Ring, Phys. Rep. **409**, 101 (2005).
- [11] J. Meng, H. Toki, S. G. Zhou, S. Q. Zhang, W. H. Long, and L. S. Geng, Prog. Part. Nucl. Phys. **57**, 470 (2006).
- [12] D. Vretenar, Nucl. Phys. A **751**, 264c (2005).
- [13] H. Kucharek and P. Ring, Z. Phys. A **339**, 23 (1991).
- [14] T. Gonzalez-Llarena, J. L. Egido, G. A. Lalazissis, and P. Ring, Phys. Lett. B **339**, 23 (1991).
- [15] D. Hirata, K. Sumiyoshi, I. Tanihata, Y. Sugahara, T. Tachibana and H. Toki, Nucl. Phys. A **616**, 438c (1997).
- [16] L. Geng, H. Toki, and J. Meng, Prog. Theor. Phys., **113**, 785 (2005).
- [17] J. Dobaczewski, H. Flocard, and J. Treiner, Nucl. Phys. A **422**, 103 (1984).
- [18] P.-G. Reinhard, B. K. Agrawal, Int. Jour. Mod. Phys. **E20**, 1379 (2011).
- [19] G. A. Lalazissis, D. Vretenar, P. Ring, Nucl. Phys. A **679**, 481 (2001).
- [20] G. A. Lalazissis, D. Vretenar, P. Ring, Phys. Rev. **C69**, 173011 (2004).
- [21] L. S. Ferreira and E. Maglione and P. Ring, Phys. Lett. B **701**, 508 (2011).
- [22] Y. Tian, Z. Y. Ma, and P. Ring, Phys. Lett. **B676**, 44 (2009).
- [23] Y. Tian, Z. Y. Ma, and P. Ring, Phys. Rev. C **80**, 024313 (2009).
- [24] A. V. Afanasjev and O. Abdurazakov, Phys. Rev. C **88**, 014320 (2013).
- [25] L. J. Wang, B. Y. Sun, J. M. Dong, and W. H. Long, Phys. Rev. C **87**, 054331 (2013).
- [26] Y. K. Gambhir, P. Ring, and A. Thimet, Ann. Phys. (N. Y.) **198**, 132 (1990).
- [27] P. Ring, Y. K. Gambhir, and G. A. Lalazissis, Comp. Phys. Comm. **105**, 77 (1997).
- [28] H. Abusara, A. V. Afanasjev, and P. Ring, Phys. Rev. **C85**, 024314 (2012).
- [29] G. A. Lalazissis, S. Karatzikos, R. Fossion, D. Peña Arteaga, A. V. Afanasjev, and P. Ring, Phys. Lett. **B671**, 36 (2009).
- [30] G. A. Lalazissis, T. Nikšić, D. Vretenar, and P. Ring, Phys. Rev. **C71**, 024312 (2005).
- [31] X. Roca-Maza, X. Viñas, M. Centelles, P. Ring, and P. Schuck, Phys. Rev. C **84**, 054309 (2011).
- [32] T. Nikšić, D. Vretenar, and P. Ring, Phys. Rev. **C78**, 034318 (2008).
- [33] S. E. Abgemava, A. V. Afanasjev, D. Ray, and P. Ring, in preparation.
- [34] A. V. Afanasjev and S. Shawaqfeh, Phys. Lett. **B706**, 177 (2011).
- [35] J. Erler, C. J. Horowitz, W. Nazarewicz, M. Rafalski, P.-G. Reinhard, Phys. Rev. c **87**, 044320 (2013).
- [36] M. Bender, K. Rutz, P.-G. Reinhard, J. A. Maruhn, and W. Greiner, Phys. Rev. **C58**, 2126 (1998).
- [37] A. V. Afanasjev, T. L. Khoo, S. Frauendorf, G. A. Lalazissis, and I. Ahmad, Phys. Rev. **C67**, 024309 (2003).